

Potential of SAR intensity tracking technique to estimate displacement rate in a landslide-prone area in Haridwar region, India

Atanu Bhattacharya¹ · Kriti Mukherjee¹ · Manoj Kuri² ·
Malte Vöge³ · M. L. Sharma⁴ · M. K. Arora⁵ ·
Rejinder K. Bhasin³

Received: 19 November 2014 / Accepted: 31 August 2015 / Published online: 7 September 2015
© Springer Science+Business Media Dordrecht 2015

Abstract Landslides constitute one of the major natural hazards that could cause significant loss of life and various human settlements. Mansa Devi hill near Haridwar city has encountered with such potential hazard for several years due to the instability of the slopes. Therefore, preparedness both on regional and site-specific basis at spatial level in the form of surface movements is extremely important to diminish the damage of human life and settlements. Though the surface movement measurement through field-based technique is always very accurate, this technique is time-consuming and unfeasible over a widely affected region. Therefore, areal and satellite remote sensing is gaining importance in landslide investigation due to its wide coverage. In recent years, synthetic aperture radar has already proven its potential for mapping ground deformation due to earthquake, landslide, volcano, etc. Therefore, in this study, an attempt has been made to identify the potential landslide-affected region in Mansa Devi area using one multi-temporal SAR technique and intensity tracking technique. Intensity tracking technique has identified significant mass movement in the landslide-affected region where the other conventional multi-temporal technique, SBAS, fails. An error analysis has been carried out in order to demonstrate the applicability of intensity tracking technique. This study demonstrated that intensity tracking can be considered as an alternative to conventional interferometry for the estimation of land surface displacement when latter is limited by loss of coherence due to rapid and incoherent surface movement and/or large acquisition time intervals between the two SAR images.

✉ Atanu Bhattacharya
atanudeq@gmail.com

¹ Institute for Cartography, Technical University Dresden, Dresden, Germany

² Civil Engineering Department, Indian Institute of Technology Roorkee, Roorkee, India

³ Norwegian Geotechnical Institute, Oslo, Norway

⁴ Earthquake Engineering Department, Indian Institute of Technology Roorkee, Roorkee, India

⁵ PEC University of Technology, Chandigarh and Indian Institute of Technology Roorkee, Roorkee, India

Keywords Synthetic aperture radar (SAR) · SAR interferometry (InSAR) · Small baseline subset (SBAS) · Intensity tracking · Landslide

1 Introduction

Landslide is one of the most dangerous threats to the population of the Indian Himalayas. Landslides and other mass movements are serious geo-environmental hazards in the Himalayas (Bhasin et al. 2002). Many villages and vital transport routes are endangered by landslides and losses of lives and important infrastructure are not uncommon. Therefore, the landslide incidences have been of serious concern to the society. It has been estimated that the annual economic losses due to landslide damages alone in the Himalayan region exceed 1 billion US dollars, including hundreds of human fatalities. (Dahal et al. 2009). Therefore, monitoring the mass movement of the land surface is an important task in order to identify potential landslide-affected area. However, due to large spatial extent of affected areas, field surveys may not be feasible. Further, estimation of repetitive displacement through field surveys at spatial level may be difficult. This may hamper the planning and monitoring processes. In areas where large landslides cannot be stabilized and may accelerate suddenly, space-based remote sensing is often the only solution to monitor the mass movement of the land surface. Therefore remote sensing and GIS based technique are used extensively to landslide application worldwide (Saha et al. 2005; Kundu et al. 2013; Pradhan 2011; Pradhan and Lee 2010; Pradhan et al. 2010, etc.). Though the availability of high-resolution optical sensors has provided enormous thrust to the landslide research, meteorological conditions such as clouds and fog and restrictions on time of imaging sometimes make it difficult to fully exploit these sensors.

To overcome these difficulties, radar remote sensing, which allows mapping irrespective of meteorological conditions both day and night, has gained its importance. Among them, InSAR technique appears to be most attractive for detecting small-to-large mass movement due to different natural and man-made hazards such as earthquakes (Massonnet et al. 1994; Fialko et al. 2001; Jonsson et al. 2002; Pathier et al. 2003; Wright et al. 1999; Bhattacharya et al. 2012a, 2013, 2014, etc.), landslides (Fruneau et al. 1996; Rott et al. 1999, etc.) and mining subsidence (Wright et al. 1999; Michaela et al. 2003; Bhattacharya et al. 2012b, etc.). First InSAR applications to measure slope motion have been reported by Fruneau et al. (1996) for a landslide (Saint-Etienne-de-Tinee) in southern France. After that, numerous studies have been carried out by several researchers around the globe (Rott et al. 1999; Rizzo and Tesauro 2000; Nagler et al. 2002; Squarzone et al. 2003; Bernardino et al. 2003; Colesanti et al. 2003; Rott and Nagler 2006; Bovenga et al. 2006; Colesanti and Wasowski 2006; Yin et al. 2010; Bovenga et al. 2012, etc.). Though DInSAR technique looks promising to monitor slope motions, several researchers have highlighted some limitations due to the atmospheric variability and the temporal decorrelation (Ding et al. 2008). Several algorithms have been used to mitigate the atmospheric effect in DInSAR processing. Among them, permanent scatterer SAR interferometry (PSInSAR) and small baseline subset (SBAS) have proved to be effective in estimating deformation at intermittent time periods in various regions around the globe. PSInSAR is based on identification of stable image pixels that are coherent over long time intervals in a stack of interferograms generated with the same master image (Ferretti et al. 2000; Hooper et al.

2004). On the contrary, SBAS uses SAR image combinations with short spatial and temporal baseline to reduce the effects of spatial and temporal decorrelation (Berardino et al. 2002; Hooper 2008, etc.). These two multi-temporal techniques have been used in various studies to detect small to rapid surface movement due to different natural disasters (Hilley et al. 2004; Colesanti and Wasowski 2006; Lauknes et al. 2010; Bhattacharya et al. 2013, 2014, etc.). PSInSAR has been found to be appropriate in urban areas where man-made structures such as bridges and high-rise buildings act as strong persistence scatterers; however, fails in areas covered with thick vegetation like mountainous region. The SBAS algorithm has been optimized for the distributed scattering mechanism where several adjacent resolution cells represent the same physical deformation phenomenon (Lauknes et al. 2010) and therefore appears appropriate in estimation of surface displacements in the thick vegetated area. However, for loss of coherence, because of thick vegetation, unreliable phase unwrapping sometimes affect this technique. Recently two image-to-image patch offset techniques, known as feature tracking technique, have been developed to monitor displacement which can minimize the limitations associated with the conventional multi-temporal techniques (Strozzi et al. 2002). Most of the applications till date are, however, still limited to measure the glacier flow only (Strozzi et al. 2002; Pritchard et al. 2005; Quincey et al. 2009; Huang and Li 2011; Jiang et al. 2012; Holt et al. 2013, etc.). To the best of our knowledge, very limited landslide studies, using only X-band SAR data, have been conducted by offset measurement technique (Raucoules et al. 2013; Singleton et al. 2014).

The feature tracking technique can be classified as intensity tracking, based on patch intensity cross-correlation optimization, and coherence tracking, based on patch coherence optimization. Though InSAR can be considered as the most accurate technique to measure the displacement in slant range direction with very high spatial resolution, most of the time it is difficult to fully exploit this technique due to loss of coherence and the reduced feasibility of phase unwrapping. Reliable phase unwrapping is only possible for areas of high coherence. In some cases, disconnected areas of high coherence separated by areas of low coherence cannot be properly analyzed (Strozzi et al. 2002). Moreover, InSAR can only estimate the displacement in slant range direction, whereas feature tracking can estimate displacement in both range and azimuth directions. Like InSAR, coherence tracking is also suitable for areas of high coherence, but the accuracy and resolution of coherence tracking are poorer than those of InSAR. Moreover, long processing times are required to track the motion of large areas at high spatial resolution. However, intensity tracking has several advantages over conventional InSAR and coherence tracking. Atmospheric disturbances and cloud cover cannot affect the SAR intensity but can affect the phase considerably. Another big advantage of using intensity information is that it is not affected by coherence due to change of vegetation cover (Strozzi et al. 2002). Moreover, SAR intensity is not affected by the signal saturation due to high displacement. Therefore, in most of the vegetated areas such as Mansa Devi, the successful analysis of SAR image pairs with large acquisition time intervals is restricted to intensity tracking. This is particularly important to exploit most of the archive data, since all the previous and current SAR missions have a long revisiting time. Though this technique has gained its reliability due to the presence of ionospheric disturbances, sometimes erroneous offset estimation in azimuth direction can be identified. However, Raucoules et al. (2013) demonstrated that longer wavelength radar signals (L-band) are mainly affected by such ionospheric disturbances. It is thus assumed that the results obtained by using C-band data are less affected by ionospheric disturbances.

Mittal et al. (2011) reported that during the monsoon season of 1998 to 2000, a major landslide along with a number of small-scale isolated landslides and rock falls occurred on the slopes of the Mansa Devi hill. However, before 2006, no such continuous monitoring of the landslide or slope instability has been done for this area. Therefore, in this study, an attempt has been made to identify the affected areas using intensity tracking and SBAS techniques and also to demonstrate the potential of intensity tracking technique by using ERS-1/2 C-band SAR data to identify landslide-related mass movement. The results obtained from SBAS and intensity tracking have also been compared for stable and landslide-affected region. Finally, an error analysis has been carried out in order to demonstrate the acceptability of intensity tracking technique for landslide application.

2 Study area

Mansa Devi hill is located near the city of Haridwar. The study area is located between longitude $77^{\circ}59'30''\text{E}$ and $78^{\circ}12'30''\text{E}$ and latitude $29^{\circ}57'30''\text{N}$ and $30^{\circ}02'00''\text{N}$ in the Haridwar district of Uttarakhand (Fig. 1). It is one of the several landslide-prone areas in Uttarakhand. The landslide area became active a decade ago and threatens the larger part of the city of Haridwar and a stretch of about 300 m of the Haridwar bypass road. Railway track, residential and commercial establishments are situated all along the base of the hill. Historically, the Mansa Devi hill has witnessed many small-to-large landslides along the slopes of the Mansa Devi hill (Gupta et al. 2013). They pose a danger to the intensively built-up areas that have developed along the foothills and in the adjoining areas on and around Mansa Devi hill, specifically along the Bhimgoda road, Haridwar. The area comes under subtropical climate with moderate to heavy rainfall during monsoon. About 70 % of the rain occurs during July to September, and moderate to heavy rainfall also occur during January and February. The study area also has been affected by severe tectonic movement (Bhattacharya et al. 2013, 2014) which have occurred along the Bhimgoda Thrust, Ganga Tear Fault and several other minor faults located in the vicinity of the study area (Bartarya et al. 2007). It has been reported that the continuous seepage of water from channels located in immediate vicinity of this area is continuously undergoing slow mass movement which indicates that mass has been mobilized by increase in pore water pressure over years (Mittal et al. 2011).

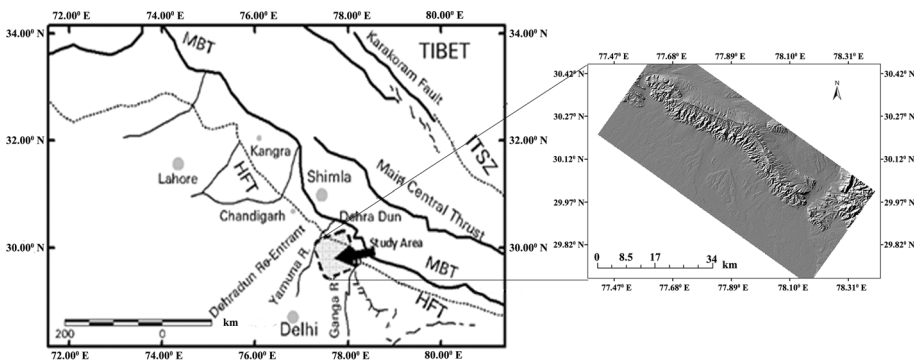


Fig. 1 Areal extent and DEM of the study area. *Rectangular box* represents the approximate extent of the SAR images

3 Data selection

The criteria for effective data selection are very critical for such kind of study and may vary widely from one technique to another. The SBAS technique is generally used to capture slow mass movement, and requires sufficient number of data to properly exploit these techniques. On the other hand, intensity tracking is used to capture rapid mass movement, so to capture the slow land mass movement image pair having long temporal baseline should be used. Keeping the above-mentioned criteria in mind, the best possible available archive dataset has been selected for this study as described in the following paragraphs in detail.

A total of 25 ERS-1/2 SAR raw images from 1992 to 2004 from descending orbit covering the study area have initially been selected for SBAS study. There were no archive data available in the year 1994, 1995 and 2001. Finally, from these 25 images, only 19 images from 1992 to 1998 have been selected based on the small perpendicular baseline criteria of 250 m. On the other hand, in order to effectively capture the slow mass movement, one image for each year from 1992 to 2004 has been selected for intensity tracking.

PSInSAR is another effective multi-temporal technique which can be used for this study. However, the data gaps for the year 1994, 1995 and 2001 of ERS stacks would affect considerably in the PSInSAR processing. Moreover, if longest continuous section from these dataset would have been considered, only 13 images could take part in the processing (1992–1993). This is insufficient for PSInSAR processing, where minimum 30 images are required to exploit this technique properly (Ferretti et al. 2000; Lauknes 2004). Therefore, PSInSAR technique has been excluded from this study. The detailed description of the datasets is given in Table 1.

Apart from SAR images, Shuttle Radar Topographic Mission (SRTM) digital elevation model (DEM) has been used to remove the topographic phase. The state vector information, instantaneous position and velocity of the satellite components expressed in Earth-centered Cartesian coordinate system have been used in this study to convert the raw data to single-look complex (SLC) data. These are necessary because the number of state vectors provided with the image data might be insufficient and imprecise for correct processing or cover an area that is too small compared to the length of the image to be processed. For ERS data, two types of orbital information from external sources are available: DELFT orbits provided by DEOS and PRC precision orbits provided by DLR. To extract state vectors from ERS-1 and ERS-2 PRC precision orbit, state vector files have been used in this study. The PRC data are available from an ftp server in Germany with a delay of about 1 month after data acquisition by ERS.

4 Brief description of the methods

In the following section, a brief methodology of SBAS and intensity tracking techniques has been described for the sake of completeness of the manuscript. For detailed description, several literatures are available and may be referred.

4.1 Small baseline subset (SBAS)

The small baseline methods are optimized for the distributed scattering mechanism, where several adjacent resolution cells represent the same physical deformation phenomenon. The basic concept behind the SBAS algorithm is to minimize the atmospheric artefacts and

Table 1 ERS-1/2 scenes of Mansa Devi area used for SBAS and intensity tracking technique

ERS-1/2 scenes used in SBAS processing				ERS-1/2 scenes used in intensity tracking	
Date	B_{PERP} (m)	B_{TEMP} (days)	No of SBAS interferograms	Date	B_{TEMP} (months)
1992-05-22	−1364	−1458	0	1992-05-22	19
1992-07-31	156	−1388	6	1993-12-03	
1992-09-04	307	−1353	6	1993-12-03	34
1992-10-09	450	−1318	4	1996-10-07	
1992-11-13	−269	−1283	3	1996-10-07	4
1992-12-18	−1683	−1248	0	1997-02-24	
1993-02-26	336	−1178	5	1997-02-24	12
1993-04-02	345	−1143	4	1998-02-09	
1993-06-11	−485	−1073	2	1998-02-09	16
1993-08-20	−473	−1003	2	1999-06-14	
1993-10-29	473	−933	2	1999-06-14	37
1993-12-03	574	−898	0	2003-07-28	
1996-02-04	169	−105	2	2003-07-28	8
1996-04-14	297	−35	0	2004-03-29	
1996-05-19	0	0	2		
1996-06-24	−222	36	2		
1996-10-07	−611	141	1		
1997-02-24	−232	281	1		
1998-02-09	−462	631	0		

topographic errors in time chronological interferograms, and to obtain multi-temporal deformation information. Interferograms with a short spatial baseline are combined, in order to minimize the spatial decorrelation. To achieve deformation time series information from multiple interferograms, the SBAS algorithm estimates the mean deformation rate and the topographic error. The atmospheric artefacts are mitigated through spatial low-pass and temporal high-pass filtering of interferograms. Most of the time, the interferograms are not adjacently linked (there may be temporal overlap or underlap between them). Therefore, SBAS uses the singular value decomposition (SVD) approach based on a minimum norm criterion of the deformation rate to derive time series deformation measurements. The basic flow diagram of the SBAS technique is shown in Fig. 2. For more details on descriptions of SBAS technique, one can refer Berardino et al. (2002), Casu et al. (2006), Lanari et al. (2007), etc.

4.2 Intensity tracking

Intensity tracking is one type of feature tracking technique where normalized cross-correlation of certain samples of master SAR intensity image is estimated with chips from the corresponding search area of a slave image. The location of the peak of the two-dimensional cross-correlation function yields the image offset. Due to thick vegetation, it is much more robust approach to estimate intensity values resulting from backscatter from

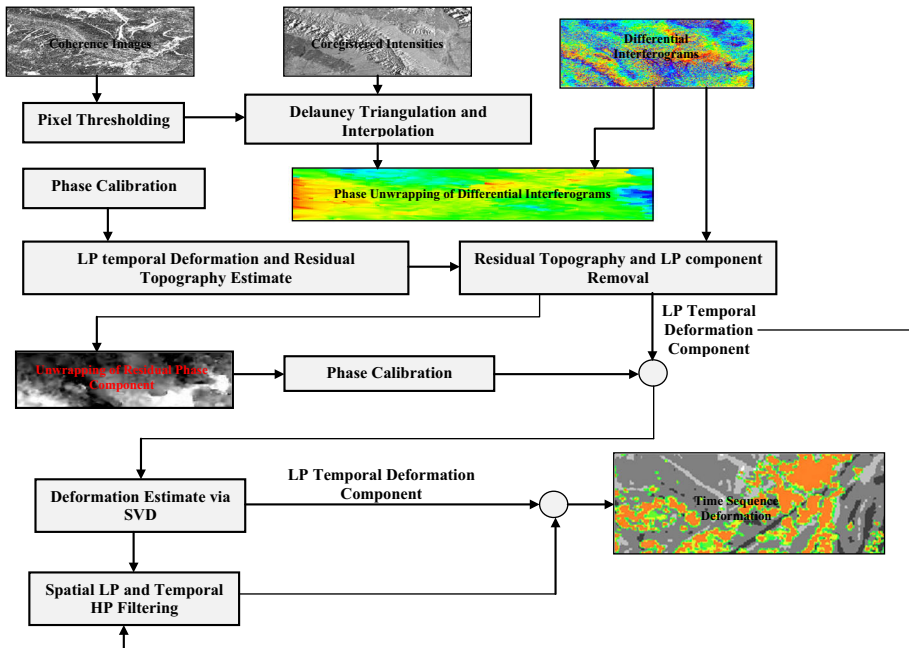


Fig. 2 SBAS workflow for displacement estimation

prominent surface features. In this technique, the registration offsets, in both slant range and azimuth directions, of two SAR images are generated and used to estimate the displacement (Strozzi et al. 2002; Pritchard et al. 2005). The estimated offsets are unambiguous values which mean that there is no need for phase unwrapping (Strozzi et al. 2002). Therefore, this technique is free from some difficult steps involved in SAR interferometry which are generally most prone to errors.

Intensity tracking method can be performed by following steps: initial estimation of the offset, determination of the bilinear polynomial function for both directions in order to co-register master and slave image with sub-pixel accuracy, precise estimation of the offsets in range and azimuth directions using normalized cross-correlation and then computation of the velocity map in range and azimuth directions.

The first coarse shift is based on the orbital data and the provided DEM. If the orbital data are not provided or do not suffice accuracy requirements, a large central window is used instead. For the second shift, a cross-correlation function is calculated which optimizes the result to a sub-pixel accuracy. This is done by defining a grid of small windows on the master image. For each window, an individual cross-correlation function is calculated. The maximum of this function is refined by oversampling of the data and is finally taken to compute the residual shift.

After the co-registration is done successfully and images are superimposed to sub-pixel accuracy, the estimation of the shift between displaced features can be started. The calculation relies on a normalized cross-correlation of small image patches that are X (range) and Y (azimuth) pixels at a set of positions in the scene. The normalized cross-correlation coefficient (NCC) of intensity image chips (Nagler et al. 2012) is given by Eq. (1)

$$NCC(M, N) = \frac{\sum_{x,y} [f(x, y) - \bar{f}_{M,N}] [t(x - M, y - N) - \bar{t}]}{\sqrt{\sum_{x,y} [f(x, y) - \bar{f}_{M,N}]^2 \sum_{x,y} [t(x - M, y - N) - \bar{t}]^2}} \quad (1)$$

where f is the intensity value of master image, t is the intensity value of reference window with pixel position at (M, N) and (x, y) is the pixel position in the reference image. \bar{t} and $\bar{f}_{M,N}$ are the mean intensity values of the reference and master window, respectively. The NCC is calculated in a regular range grid and calculated image offsets in both range and azimuth directions. To get the correct offset value, the algorithm searches for the location of the highest peak within the cross-correlation function (Fig. 3). To increase the accuracy, the data are additionally oversampled. The potentiality of this technique depends on the existence of identical and distinguishable characteristics in intensity data that are easily identified within the image patch under comparison (Strozzi et al. 2002).

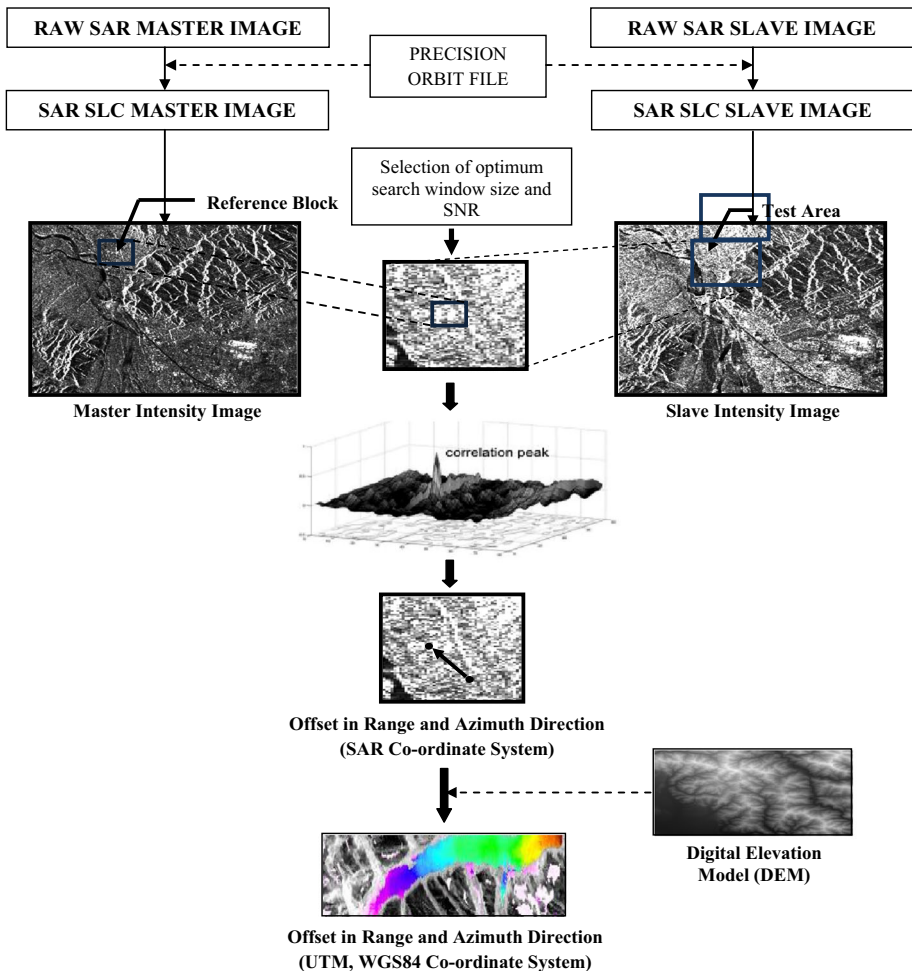


Fig. 3 Flow chart of offset estimation in range and azimuth directions using intensity tracking technique after Käab and Vollmer (2000)

5 Data processing and results

5.1 SBAS data processing and results

In SBAS processing, a total of 42 interferograms have been constructed from 19 images using a threshold of 250-meter perpendicular baseline and 4-year temporal baseline (Bhattacharya et al. 2014). It can be assumed that the SAR scenes that are weakly linked, i.e., long perpendicular baseline and large temporal baseline, are more susceptible to unwrapping errors. Therefore, two images (May 22, 1992, and December 18, 1992) with extreme baselines have been excluded, thereby reducing the number of images being used in the study from 19 to 17. The overall processing has been performed by applying a complex multi-look operation. For each complex interferogram, the best-fitting linear phase ramp due to imprecise orbit knowledge has been estimated and removed (Berardino et al. 2002). Then in de-trending process, the phase delay elevation profile for each interferograms has been estimated and a linear inversion has been used to obtain the phase delay profiles for each dataset. After de-trending, out of 42 interferograms, 20 interferograms, where distinct fringes were visible, have been selected visually for SBAS processing.

In order to eliminate de-correlated areas from the study and to make phase unwrapping more robust, a pixel thresholding technique has been adopted (Berardino et al. 2002). About 284,763 pixels have been identified which exhibit coherence higher than 0.3 in at least 30 % of the computed interferograms. Freely available phase unwrapping software, Statistical Cost Network Flow Algorithm for Phase Unwrapping (SNAPHU), developed by Stanford University (Chen and Zebker 2001) has been used for phase unwrapping purpose. Since the phase unwrapping operation has been applied only to the pixels that exhibit a coherence value greater than the coherence threshold, to join all the sparse data a Delauney triangulation interpolation has been used (Lauknes et al. 2010). After phase unwrapping, the phase has been calibrated with respect to one high-coherence pixel located in a stable area.

Next the atmospheric effect is eliminated using a filtering operation. For this, a space-time filtering operation has been performed on each selected pixel as described in Bhattacharya et al. (2014). Once the atmospheric component has been estimated by filtering operation, it is subtracted from the estimated phase signal. In the next step, the velocity map has been estimated using L_2 -norm-based SVD decomposition method (Berardino et al. 2002). Figure 4 shows the estimated mean LOS velocity map in mm/year. The LOS velocity values have been obtained for those pixels which have been selected through coherence threshold. For the velocity map, it can be seen that the reliable coherence has been achieved in the urban area of Haridwar and along those parts of the riverbed with only sparse vegetation. The mountain range to the western part of the city shows very poor to no coherence, so that no displacements could be measured in the areas near landslide-affected area.

It is very difficult to infer any conclusion from these results because most of the displacement signal covers the non-landslide area. However, three points, shown in Fig. 4, have been selected to understand the displacement nature of this study area. The relative displacements of point 1 and point 2 with respect to point 3 have been studied. Subtracting the velocity offset of point 3, which was about 6 mm/year, a slightly negative displacements of point 1 and point 2 (Fig. 5) have been observed. However, the reliability of these displacement magnitudes cannot be estimated with full confidence due to the less spatial extent of the detected area and low coherence. Though it is known that the detected area, in

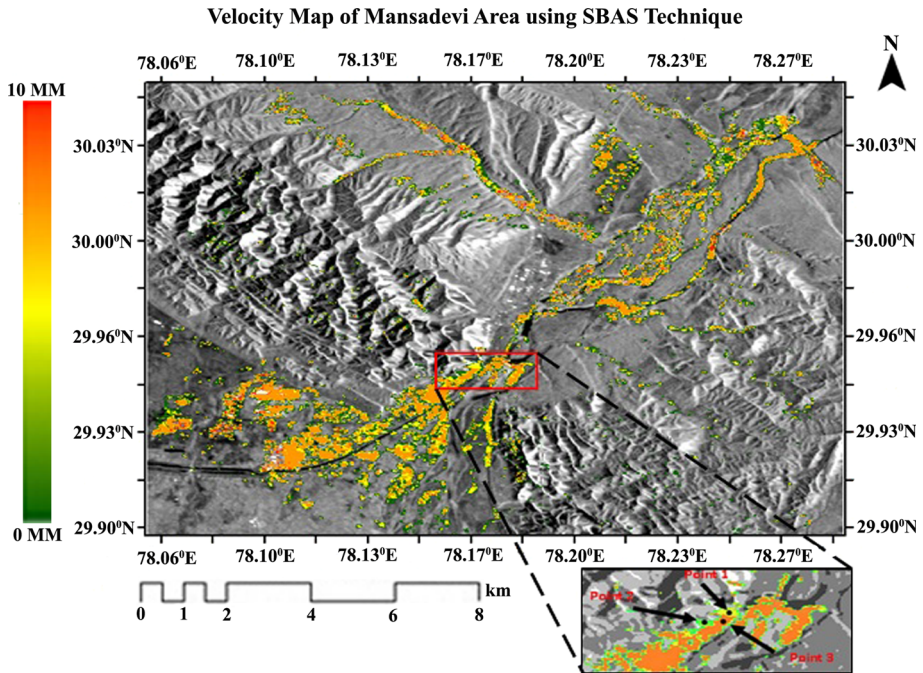


Fig. 4 Mean velocity map for the ERS image stack (1992–1998) using SBAS over Mansa Devi

fact, was prone to small-scale landslides in the year 2011 (Vöge et al. 2015) (Fig. 6), based on the initial results we cannot deduce whether these slides were caused by a larger deformation mechanism which started decades ago or just purely rain-induced small mass movement. Therefore, due to low coherence in mountainous region, SBAS technique has not been able to produce any strong evidence of surface movement in Mansa Devi hill slope.

5.2 Intensity tracking data processing and results

Intensity tracking has been employed to ERS-1/2 data from 1992 to 2004 to retrieve displacement values in Mansa Devi region. For each year, one ERS data have been selected for intensity tracking. In order to compute the initial co-registration offset, precise orbit information has been used.

Initial co-registration has been performed in two subsequent stages, i.e., coarse and fine registrations. In coarse registration, the offsets in azimuth and range direction are calculated using orbit information (Small et al. 1993), and then cross-correlation intensity (CCI) algorithm is used in fine registration. In this study, a set of image chips of sizes 64×64 have been selected and the initial offsets from coarse registration have been determined (Small et al. 1993). After offset estimation, a 4-parameter model in range and azimuth directions has been developed using least squares (LS) analysis (Small et al. 1993). To perform the LS analysis, pixels having signal-to-noise ratio (SNR) greater than 7.0 have been identified using a 64×64 pixel correlation search windows of 24×24 pixels in range and azimuth directions, respectively.

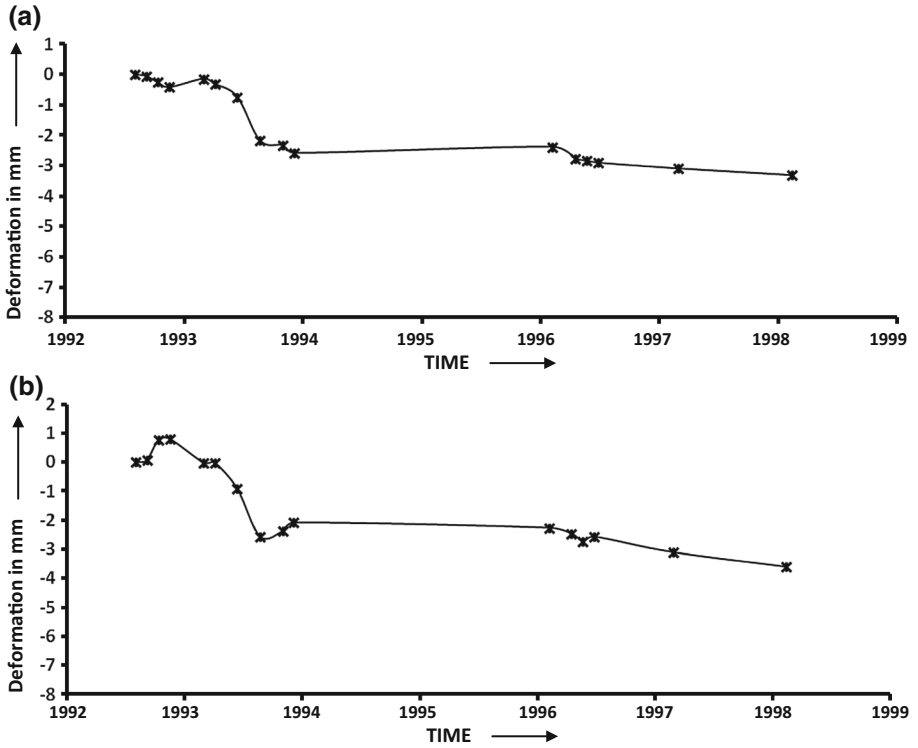


Fig. 5 Displacement time series of a point 1 and b point 2 with respect to point 3 of Mansa Devi area

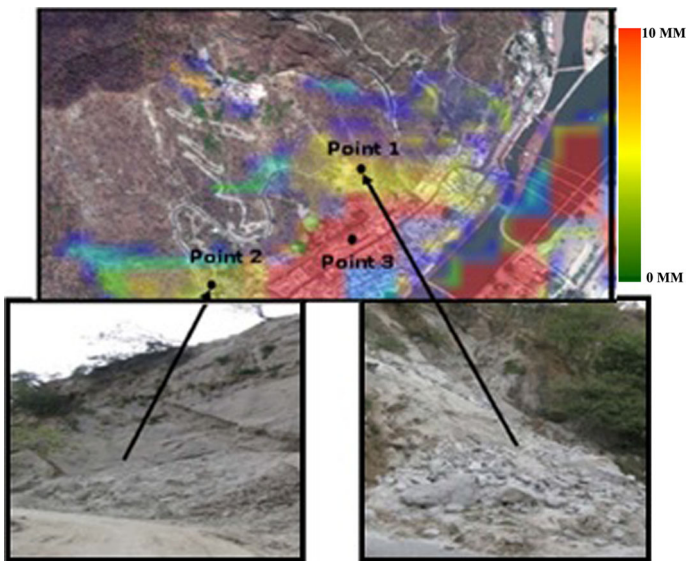


Fig. 6 Two small landslides that had occurred in 2011 at the identified locations in the Mansa Devi area (picture taken during field visit)

After the co-registration, the estimation of the shift between displaced features can be started. The calculation relies on a normalized cross-correlation of small image patches. To get the correct offset value, the algorithm searches for the location of the highest peak within the cross-correlation function. To increase the accuracy, the data are additionally oversampled by a factor 2.

For the present study with ERS SAR data, patch sizes of 64×64 and 64×128 windows have been systematically tested, which corresponds to around 1300 m by 250 and 1300 m by 500 m, respectively, in ground range and azimuth directions. The sampling interval was considered as 1×5 pixels in range and azimuth directions, respectively, which is relatively less dense, approximately 20×20 meters in ground range and azimuth, respectively, with the intention that total affected area due to mass movement could be sufficiently large. The displacement magnitude and sum of ground range and azimuth displacement are shown in Fig. 7a–g for all the ERS pair.

The displacement has been measured in two directions, i.e., ground range direction and azimuth direction. However, due to the unavailability of ground truth data, the displacement magnitude has not been directly compared. Several error analyses have been performed and discussed in order to check the processing results. However, it is clearly visible from the Fig. 7 that the intensity tracking technique could estimate displacement in areas which exhibited low coherence due to thick vegetation in Mansa Devi area. It has been reported that during the monsoon season of 1998, a major landslide and several moderate landslides activities during 1998 to 2000 have occurred in this region (Mittal et al. 2011). Moreover, slightly high displacement value in northwestern part of the Mansa Devi Temple also can be observed from displacement magnitude images (Fig. 9). Various small- and medium-size landslides can also be identified from Google image in this region.

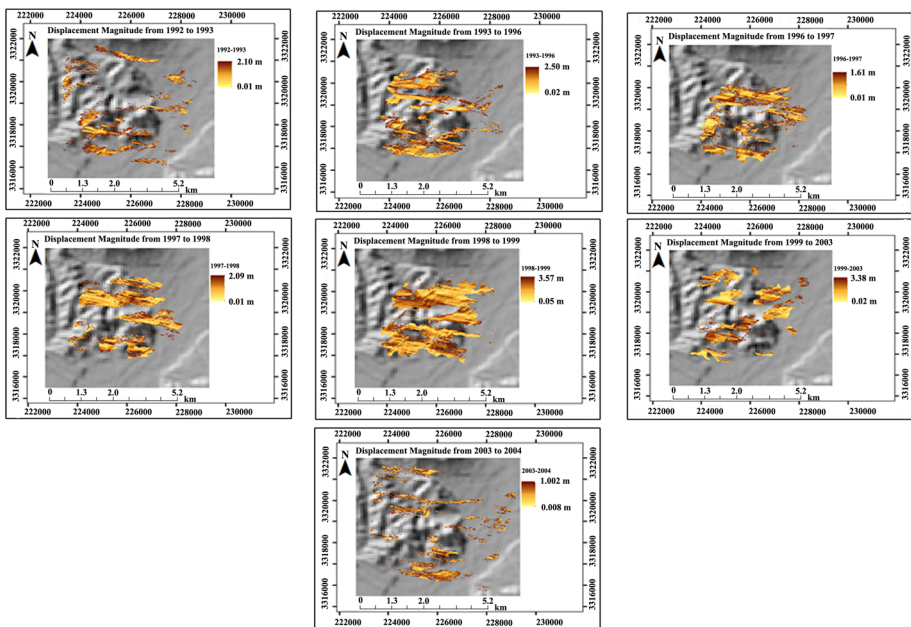


Fig. 7 Displacement magnitude of all ERS-1/2 pairs using intensity tracking **a** 1992–1993, **b** 1993–1996, **c** 1996–1997, **d** 1997–1998, **e** 1998–1999, **f** 1999–2003 and **g** 2003–2004

Though in order to understand the landslide activities at a finer scale, a long-term observation along with a ground-based monitoring is needed, intensity tracking technique can be considered as an effective tool to recognize and identify new and existing landslides in complex steep mountain region.

6 Comparison of the results

Though SBAS technique is very useful for determining ground displacement (Bhattacharya et al. 2014), due to several unfavorable conditions this technique failed to produce any displacement signal in the landslide-prone area. In the next paragraph, several possible factors affecting the results of SBAS processing have been identified.

In order to exploit the SBAS technique in low-coherence area, it has been recommended that at least 25–30 images should be used (Lauknes 2004). In this study, however, among 19 available images, two images, acquired on May 1992 and December 1992, have been excluded from the dataset due to very low coherence. Further, in interferogram selection stage, another image (July 1996) has also been excluded by visual inspection. Thus, a total of 16 images could be effectively used in the processing which is considered to be still less as compared to the recommended number of image for SBAS. Moreover, the irregular sampling, absence of available images in the period between 1994 and 1996 also affected the results especially in phase unwrapping stage. Further, the number of interferogram combinations also improves the stability of the method since possible phase unwrapping errors can be mitigated due to the data redundancy. It can be expected that if few interferograms are computed with respect to a particular SAR scene, the SVD inversion will be less robust and the noise level will be high (Lauknes 2004). It can be observed from Table 1 that number of SBAS interferogram combinations was very limited for most of the images. Another important step of SBAS method is the requirement of phase unwrapping and this leads to ambiguity error into the final result. On the other hand, the offset estimated in intensity tracking is unambiguous which mean that there is no need for phase unwrapping (Strozzi et al. 2002). Therefore, this technique is free from most erroneous and difficult steps in SAR interferometry. In addition, displacement in azimuth direction obtained from intensity tracking procedure can be combined with slant range displacement obtained from any DInSAR procedure in order to retrieve a two-dimensional displacement map when SAR data of only one orbit configuration are available.

The results of SBAS and intensity tracking method have finally been compared in some positions from stable as well as landslide-prone area. SBAS can detect the displacement in radar line of sight or slant range direction, whereas intensity tracking can detect displacement in 2D displacement field such as ground range and azimuth directions. Therefore, in this study, the ground range displacement components of some randomly selected pixels in the stable terrain have been selected for comparison and are shown in Table 2. Detail procedure for generating ground range displacement component of SBAS technique has been discussed in Bhattacharya et al. (2014). The mean displacement value of those randomly selected pixels achieved from intensity tracking was slightly less as compared to the SBAS technique. However, the error associated with the displacement estimate in intensity tracking technique was relatively high as compared to SBAS technique. The reason may be because intensity tracking technique is more useful to estimate large displacement field, and in the contrary, multi-temporal InSAR like SBAS is more effective to detect slow displacement field. Therefore, the surface displacement for stable areas has been better estimated by SBAS technique.

Table 2 Comparison of SBAS and intensity tracking technique for stable and landslide-prone area

Data 1	Data 2	Stable area		Landslide-affected area			
		Ground range displacement using SBAS in stable area (m/year) (Bhattacharya et al. 2014)	Ground range displacement using intensity tracking in stable area (m/year) using 64 × 64 search window	Six selected points in landslide-affected region		Displacement magnitude (m/year) using SBAS technique for selected points	Displacement magnitude (m/year) using intensity tracking technique for selected points
				Latitude	Longitude		
19920522	19931203	0.031 ± 0.004	0.009 ± 0.079	29.96417	78.17245	No displacement signal	0.45 ± 0.021
19931203	19961007		0.008 ± 0.075	29.96778	78.16760		0.60 ± 0.029
19961007	19970224		0.010 ± 0.070	29.96657	78.16835		0.56 ± 0.026
19970224	19980209		0.012 ± 0.060	29.96612	78.16917		0.47 ± 0.011
19980209	19990614		0.007 ± 0.070	29.96967	78.16842		0.60 ± 0.105
19990614	20030728		0.012 ± 0.100	29.96885	78.16887		0.49 ± 0.370
20030728	20040329		0.011 ± 0.079				

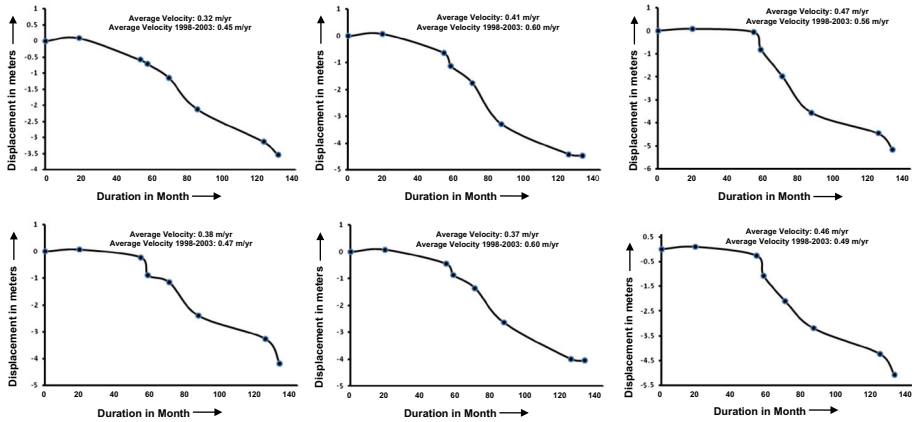


Fig. 8 Displacement in ground range direction of some selected pixels in the landslide-affected region (negative sign indicated away from the satellite)

Moreover, in order to examine the displacement behavior, some points have been selected from the area which were identified as mostly affected region by the Centre of Excellence for Urban Development and Climate Change, India, during 1998 to 2000 (<https://www.scribd.com/doc/29839775/Reconnaissance-land-slide-Survey-Report-of-MNSA-Hill-Haridwar>). The ground range displacement history of such points using intensity tracking technique has been estimated and is shown in Fig. 8. However, no displacement signal could not be obtained for those points by using SBAS technique (last two columns of Table 2). It can be inferred from Fig. 8 that the average displacement rate during the year between 1998 and 2003 is much more as compared to the overall average displacement of whole time span. Therefore, the displacement estimated by intensity tracking technique also supports the reported event in Mansa Devi area.

7 Error analysis of intensity tracking technique

In order to demonstrate the applicability of intensity tracking procedures, an error analysis has been carried out (Jiang et al. 2012). The significant errors in intensity tracking have been related to the co-registration, transformation of velocity in horizontal direction and systematic errors (Strozzi et al. 2002; Nakamura et al. 2007; Jiang et al. 2012). The theoretical error of offset in the horizontal direction caused by co-registration is shown in the following equation:

$$E_h = \frac{2(\text{Range offset} \times \delta_{\text{Range}} + \text{Azimuth offset} \times \delta_{\text{Azimuth}})}{\sqrt{\text{Range offset}^2 + \text{Azimuth offset}^2}} \tag{2}$$

where E_h is the theoretical error in the horizontal direction, δ_{Range} is the standard deviation of co-registration in the range direction and δ_{Azimuth} is the standard deviation of co-registration in the azimuth direction. In order to calculate the error associated with intensity tracking processing, the standard deviation of the final polynomial model fit in ground range and azimuth directions has been estimated for all pairs of data and is shown in Table 3. It has been observed that for most of the cases, the theoretical errors of offset in

Table 3 Theoretical error of offsets in horizontal directions for all data pairs used in intensity tracking technique (64×64 search window size)

No	Data 1	Data 2	64×64 search window size					
			Range offsets (pixels)	Azimuth offsets (pixels)	SD in co-registration in range (pixels)	SD in co-registration in azimuth (pixels)	Theoretical error of offsets in horizontal direction given in Eq. (2) (pixels)	Sum of range and azimuth errors (pixels)
1	19920522	19931203	9.72	9.77	0.028	0.069	0.137	0.097
2	19931203	19961007	14.11	14.84	0.035	0.091	0.180	0.126
3	19961007	19970224	4.15	21.43	0.022	0.056	0.118	0.078
4	19970224	19980209	13.74	12.89	0.028	0.068	0.133	0.096
5	19980209	19990614	21.16	22.58	0.031	0.081	0.160	0.112
6	19990614	20030728	4.12	38.39	0.037	0.115	0.236	0.152
7	20030728	20040329	7.58	8.07	0.027	0.086	0.162	0.113

horizontal direction, as given in Eq. (2), are larger than $\sqrt{2}$ times the sum of the range and azimuth errors (last column of Table 3), and less than two times of either the range or azimuth errors. Strozzi et al. (2002) suggested that the theoretical error in horizontal direction can be considered as roughly the sum of the errors in range and azimuth directions, respectively. This assumption has been considered in this study to estimate the theoretical errors of intensity tracking.

However, the theoretical error is not the true error associated with the processing (Jiang et al. 2012). True error can be estimated by analyzing the processing results in stable area (Jiang et al. 2012) which also neglect the effect of systematic noise and the ionospheric effects (Strozzi et al. 2002; Pritchard et al. 2005). In glacier study, the non-glaciated regions or the areas nearly 100 m away from rivers have been considered as stable area (Jiang et al. 2012). However, in this study, higher-coherence pixels in urban areas have been considered to represent for near-stable area. These pixels have been designated as near stable because negligible displacement has already been observed by several studies (Bhattacharya et al. 2012a, 2013, 2014). The mean and standard deviation (true error) values of such stable (nearly 360,000) pixels have been calculated and are shown in Table 4. The theoretical errors for the stable areas also have calculated using the method referred to Strozzi et al. (2002) and are shown in Table 4. For example, the theoretical error of the 1992–1993 pair has been computed as 0.31 m per year, which has been obtained as $7.9 \times 0.028 + 3.99 \times 0.069 = 0.49$ m in 19 months (equivalent to 0.31 m per year). The pixel size of ERS-1/2 data is roughly 7.9 and 3.99 m in range and azimuth directions, respectively. The standard deviation of the final polynomial model fit in ground range and azimuth directions, as shown in Table 3, has been estimated as 0.028 and 0.069, respectively. For all other datasets, the theoretical errors have calculated in the same manner. It has been observed that the theoretical errors are considerably high as compared to the true error. This may be due to the fact that the theoretical error has been calculated by using the standard deviation of the final polynomial model fit of high SNR pixels of the overall image in range and azimuth directions. Due to the thick vegetation and rugged terrain condition, less amount of pixels exhibited high SNR value; therefore, overall

Table 4 Theoretical and true errors of displacement in stable area using intensity tracking technique

No	Data 1	Data 2	Displacement using 64 × 128 search window in stable area (intensity tracking)		Displacement using 64 × 64 search window in stable area (intensity tracking)		Theoretical errors (Strozzi et al. 2002) in (m/year)
			Mean error (m/year)	True errors (m/year)	Mean error (m/year)	True errors (m/year)	
1	19920522	19931203	0.015	0.071	0.012	0.071	0.31
2	19931203	19961007	0.011	0.050	0.010	0.041	0.22
3	19961007	19970224	0.018	0.120	0.011	0.090	1.08
4	19970224	19980209	0.013	0.066	0.012	0.050	0.49
5	19980209	19990614	0.016	0.083	0.011	0.067	0.42
6	19990614	20030728	0.010	0.105	0.013	0.150	0.24
7	20030728	20040329	0.015	0.090	0.012	0.075	0.83

standard deviation of the polynomials in both directions is quite high. On the other hand, the true error has been estimated from the standard deviation of the displacement magnitude of the stable areas. It can be expected that more SNR pixels can reduce the overall standard deviation of the final polynomial model and hence the theoretical error.

The selection of search window size also considerably affects the offset estimate (Jiang et al. 2012). The search window size strongly depends upon the applications. In glacier application, several search windows (64 × 256 for Greenland glacier (Pritchard et al. 2005); 64 × 64 for surge of Monacobreen in northern Svalbard (Strozzi et al. 2002); 128 × 256 for glaciers on Karakoram Mountains (Jiang et al. 2012)) have been used depending on the nature of the glacier flow. In this study, the displacement statistics of the stable areas have been used to study the effect of the windows size. Two search windows size of 64 × 128 and 64 × 64 have been compared for all set of data. Distribution of the displacement magnitude for those stable pixels has been computed using two search windows and is shown in Figs. 9 and 10. It can be observed from the Table 4 that the results are not much affected by the choice of the search window size. However, slightly less true error value has been obtained by using 64 × 64 search window size for all datasets, except the data pair of 1999–2003. Therefore, 64 × 64 search window size has been chosen for the processing of all the datasets.

8 Conclusions

SAR multi-temporal technique such as SBAS and intensity tracking has been used in Mansa Devi hill, Haridwar region, to identify the mass movement due to landslide. Due to low coherence and insufficient effective number of dataset, the SBAS technique was not able to produce any strong evidence of surface movement in the landslide-affected region. Intensity tracking can be considered as a feasible method to identify surface movement over long acquisition time intervals due to landslide, especially for highly vegetated area like Mansa Devi hill slope. Very limited studies have exploited intensity tracking technique to observe mass movement due to landslide. In this study, it has been observed that

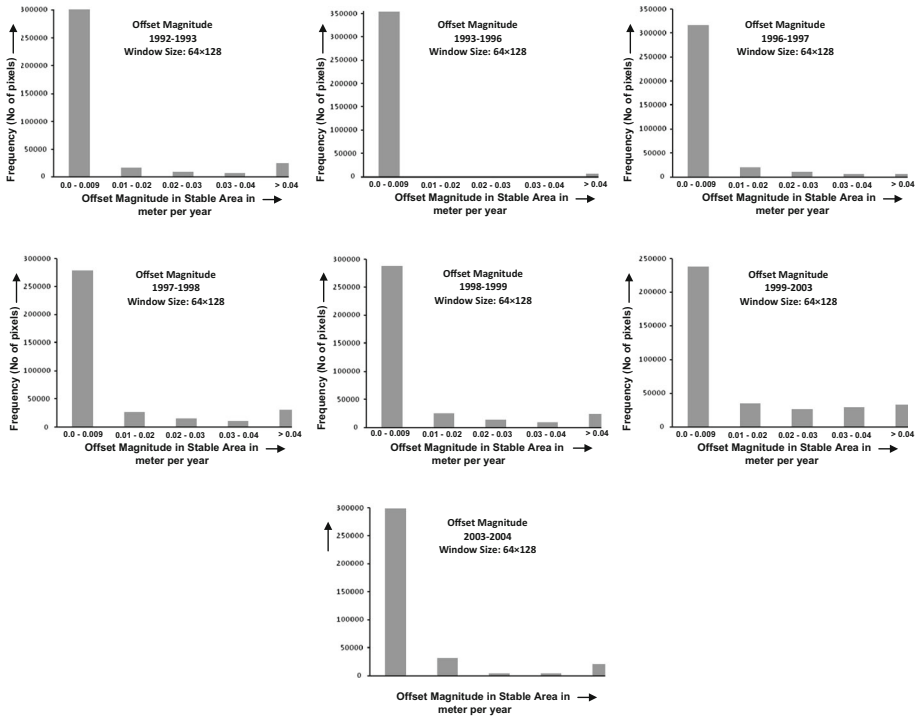


Fig. 9 Distribution of displacement magnitude over stable areas using 64×128 search window size

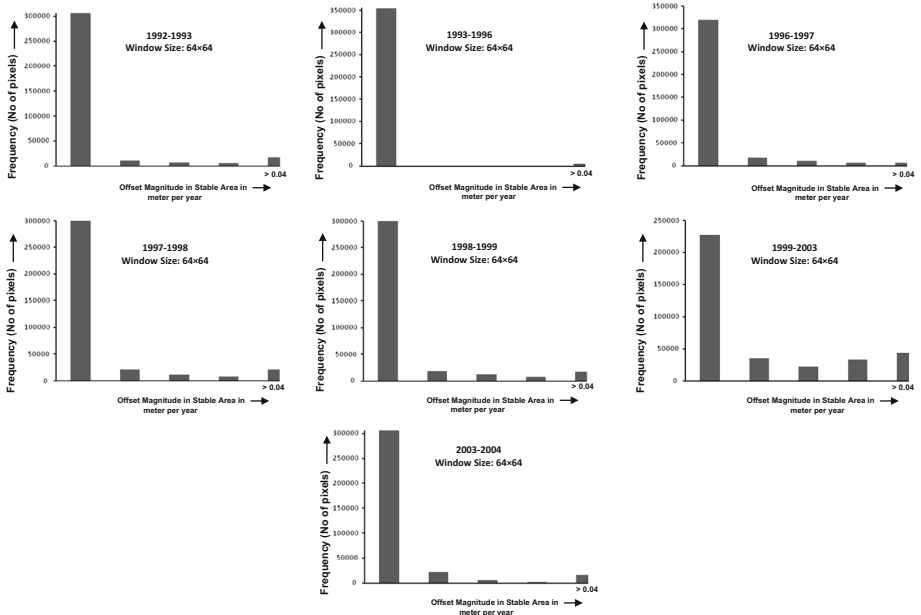


Fig. 10 Distribution of displacement magnitude over stable areas using 64×64 search window size

not only X-band data but also C-band data can be effectively used to detect the mass movement. However, due to lack of ground truth data, the results have been analyzed qualitatively. A detailed error analysis has been carried out to demonstrate the effectiveness of intensity tracking. Several portions of the images show a considerable amount of ground displacement, and various small-to-moderate landslides can be observed in these locations from other optical image sources. The displacement magnitude of intensity tracking technique also indicated a much faster displacement during 1998–2003 which agrees with the reported landslide activities in this region. Intensity tracking is particularly important to exploit most of the archive data, since all the previous and current SAR missions have a long revisiting time. Moreover, in some cases, intensity tracking is the only technique that can be applied for very large and incoherent displacements as the result of fast moving mass or large acquisition time intervals between two SAR images. Combining the range and azimuth displacement from both ascending and descending orbit has been recommended to understand the complete 3D surface velocity. To understand the landslide activities at a finer scale, a long-term observation along with a ground-based monitoring are also recommended, but intensity tracking technique can be considered as an effective tool to recognize and identify new and existing landslides in complex steep mountain region.

Acknowledgments The corresponding author would like to acknowledge the research funding from the Alexander von Humboldt (AvH) Foundation. The ERS-1/2 data have been provided by the European Space Agency. We also acknowledge the helpful and constructive reviews of the anonymous reviewers.

References

- Bartarya SK, Mazari RK, Virdi NS (2007) Bhimgoda slide of August 24, 1994 in the Siwalik rocks near Haridwar: a success story of landslide control measures. In: Varma OP, Mahajan AK, Gupta V (eds) *Natural hazards: special publication of indian geological congress*, pp 155–167
- Berardino P, Fornaro G, Lanari R, Sansosti E (2002) A new algorithm for surface deformation monitoring based on small baseline differential SAR interferograms. *IEEE Trans Geosci Remote Sens* 40(11):2375–2383
- Berardino P, Costantini M, Franceschetti G, Iodice A, Pietranera L, Rizzo V (2003) Use of differential SAR interferometry in monitoring and modelling large slope instability at Maratea (Basilicata, Italy). *Eng Geol* 68:31–51
- Bhasin R, Grimstad E, Larsen JO, Dhawan AK, Singh R, Verma SK, Venkatachalam K (2002) Landslide hazards and mitigation measures at Gangtok, Sikkim Himalaya. *Eng Geol* 64:351–368
- Bhattacharya A, Sharma ML, Arora M (2012a) Surface displacement estimation along Himalayan frontal fault using differential SAR interferometry. *Nat Hazard* 64(2):1105–1123
- Bhattacharya A, Arora MK, Sharma ML (2012b) Usefulness of synthetic aperture radar (SAR) interferometry for digital elevation model (DEM) generation and estimation of land surface displacement in Jharia coal field area. *Geocarto Int* 27(1):57–77
- Bhattacharya A, Vöge M, Arora MK, Sharma ML, Bhasin RK (2013) Surface displacement estimation using multi-temporal SAR interferometry in a seismically active region of the Himalaya. *Georisk Assess Manag Risk Eng Syst Geohazards* 7(3):84–97
- Bhattacharya A, Arora MK, Sharma ML, Vöge M, Bhasin RK (2014) Surface displacement estimation using space-borne SAR interferometry in a small portion along Himalayan Frontal Fault. *Opt Lasers Eng* 53:164–178
- Bovenga F, Nutricato R, Refice A, Wasowski J (2006) Engineering, Application of multitemporal differential interferometry instability detection in urban/peri-urban areas. *Geology* 88:218–239
- Bovenga F, Wasowski J, Nitti DO, Nutricato R, Chiaradia MT (2012) Using COSMO/SkyMedX-band and ENVISAT C-band SAR interferometry for landslides analysis. *Remote Sens Environ* 119:272–285

- Casu F, Manzo M, Lanari R (2006) A quantitative assessment of the SBAS algorithm performance for surface deformation retrieval from DInSAR data. *Remote Sens Environ* 102(3–4):195–210
- Chen CW, Zebker HA (2001) Two dimensional phase unwrapping with use of statistical models for cost functions in non-linear optimization. *J Opt Soc Am A* 18(2):338–352
- Colesanti C, Wasowski J (2006) Investigating landslides with space-borne synthetic aperture radar (SAR) interferometry. *Eng Geol* 88:173–199
- Colesanti C, Ferretti A, Prati C, Rocca F (2003) Monitoring landslides and tectonic motion with the Permanent Scatterers Technique. *Eng Geol* 68:3–14
- Dahal RK, Hasegawa S, Yamanaka M, Dhakal S, Bhandary NP, Yatabe R (2009) Comparative analysis of contributing parameters for rainfall-triggered landslides in the Lesser Himalaya of Nepal. *Environ Geol* 58(3):567–586
- Ding XL, Li ZW, Zhu JJ, Feng GC, Long JP (2008) Atmospheric effects on InSAR measurements and their mitigation. *Sensor* 8:5426–5448
- Ferretti A, Prati C, Rocca F (2000) Nonlinear subsidence rate estimation using permanent scatterers in differential SAR interferometry. *IEEE Trans Geosci Remote Sens* 38(5):2202–2212
- Fialko Y, Simons M, Agnew D (2001) The complete (3-D) surface displacement field in the epicentral area of the 1999 Mw 7.1 Hector Mine earthquake, California, from space geodetic observations. *Geophys Res Lett* 28(16):3063–3066
- Fruneau B, Achace J, Delacourt C (1996) Observation and modelling of the Sant-Etienne-de Tinée landslide using SAR interferometry. *Tectonophysics* 265:181–190
- Gupta V, Asthana AKL, Mazari RK (2013) Slope instability and risk assessment of the Mansa Devi Hill near Haridwar township, Uttarakhand. *Int J Fundam Appl Res* 1(1):37–47
- Hilley GE, Burgmann R, Ferretti A, Novati F, Rocca F (2004) Dynamics of slow moving landslides from permanent scatterer analysis. *Science* 304(5679):1952–1955
- Holt TO, Glasser NF, Quincey DJ, Siegfried MR (2013) Speedup and fracturing of George VI Ice Shelf, Antarctic Peninsula. *Cryosphere* 7:797–816
- Hooper A (2008) A multi-temporal InSAR method incorporating both persistent scatterer and small baseline approaches. *Geophys Res Lett* 35(L1):6302–6306
- Hooper A, Zebker HA, Segall P, Kampes B (2004) A new method for measuring deformation on volcanoes and other natural terrains using InSAR persistent scatterers. *Geophys Res Lett* 31(23):L23611
- Huang L, Li Z (2011) Comparison of SAR and optical data in deriving glacier velocity with feature tracking. *Int J Remote Sens* 32(10):2681–2698
- Jiang ZL, Liu SY, Peters J, Lin J, Long SC, Han YS, Wang X (2012) Analyzing Yengisogat Glacier surface velocities with ALOS PALSAR data feature tracking, Karakoram, China. *Environ Earth Sci* 67:1033–1043
- Jonsson S, Zebker H, Segall P, Amelung F (2002) Fault slip distribution of the 1999 Mw 7.1 Hector Mine, California, earthquake, estimated from satellite radar and GPS measurements. *Bull Seismol Soc Am* 92(4):1377–1389
- Kääb A, Vollmer M (2000) Surface geometry, thickness changes and flow fields on creeping mountain permafrost: automatic extraction by digital image analysis. *Permafr Periglac Process* 11(4):315–326
- Kundu S, Saha AK, Sharma DC, Pant CC (2013) Remote Sensing and GIS based landslide susceptibility assessment using binary logistic regression model: a case study in the Ganeshganga watershed, Himalayas. *J Indian Soc Remote Sens* 41(3):697–709
- Lanari R, Casu F, Manzo M, Zeni G, Berardino P, Manuta M, Pepe A (2007) An overview of the small baseline subset algorithm: a DInSAR technique for surface deformation analysis. *Pure appl Geophys* 164(4):637–661
- Lauknes TR (2004) Long-term surface deformation mapping using small baseline differential SAR interferogram. Unpublished Master Thesis, Department of Physics and Technology, University of Tromsø, Norway
- Lauknes TR, Piyush Shanker A, Dehls JF, Zebker HA, Henderson IHC, Larsen Y (2010) Detailed rockslide mapping in northern Norway with small baseline and persistent scatterer interferometric SAR time series methods. *Remote Sens Environ* 114(9):2097–2109
- Massonnet D, Feigl K, Rossi M, Adragna F (1994) Radar interferometric mapping of deformation in the year after the Landers earthquake. *Nature* 369:227–230
- Michaela K, Achim R, Nico A, Bert K, Horst JN (2003) Remote sensing observation of mining induced subsidence by means of differential SAR interferometry. In: Proceedings of the international geoscience and remote sensing symposium (IGARSS'03), 21–25th July, Toulouse, vol 1, pp 209–211
- Mittal SK, Dhingra S, Sardana HK (2011) Analysis of data using neuro-fuzzy approach recorded by instrumentation network installed at Mansa Devi (Haridwar) landslide site. *J Sci Ind Res* 70:25–31

- Nagler T, Rott H, Kamelger A (2002) Analysis of landslides in Alpine areas by means of SAR interferometry. In: IEEE international geoscience and remote sensing symposium (IGARSS'02), 24–28 June 2002, Toronto, vol 1, pp 198–200
- Nagler T, Rott H, Hetzenecker M, Scharer K, Magnusson E, Floricioiu D, Notarnicola C (2012) Retrieval of 3D-glacier movement by high resolution X-band SAR data. In: IEEE international geoscience and remote sensing symposium (IGARSS'12), 22–27 July 2012, Munich, pp 3233–3236
- Nakamura K, Doi K, Shibuya K (2007) Estimation of seasonal changes in the flow of Shirase Glacier using JERS-1/SAR image correlation. *Polar Sci* 1:73–83
- Pathier E, Fruneau B, Deffontaines B, Angelier J, Chang C, Yu S, Lee C (2003) Coseismic displacements of the footwall of the Chelungpu fault caused by the 1999, Taiwan, Chi-Chi earthquake from InSAR and GPS data. *Earth Planet Sci Lett* 212(1–2):73–88
- Pradhan B (2011) Use of GIS based fuzzy logic relations and its cross application to produce landslide susceptibility maps in three test areas in Malaysia. *Environ Earth Sci* 63(2):329–349
- Pradhan B, Lee S (2010) Regional landslide susceptibility analysis using back-propagation neural network model at Cameron Highland, Malaysia. *Landslides* 7(1):13–30
- Pradhan B, Sezer EA, Gokceoglu C, Buchroithner MF (2010) Landslide susceptibility mapping by neuro-fuzzy approach in a landslide-prone area (Cameron Highlands, Malaysia). *IEEE Trans Geosci Remote Sens* 48(12):4164–4177
- Pritchard H, Murray T, Luckman A, Strozzi T, Barr S (2005) Glacier surge dynamics of Sortebræ, east Greenland, from synthetic aperture radar feature tracking. *J Geophys Res* 110:1–13
- Quincey DJ, Luckman A, Benn D (2009) Quantification of Everest region glacier velocities between 1992 and 2002, using satellite radar interferometry and feature tracking. *J Glaciol* 55:596–606
- Raucoules D, deMichele M, Malet JP, Ulrich P (2013) Time-variable 3D ground displacements from high-resolution synthetic aperture radar (SAR). application to La Valette landslide (South French Alps). *Remote Sens Environ* 139:198–204
- Rizzo V, Tesauro M (2000) SAR interferometry and field data of Randazzo landslide (Eastern Sicily, Italy). *Phys Chem Earth* 25(9):771–780
- Rott H, Nagler T (2006) The contribution of radar interferometry to the assessment of landslide hazards. *Adv Space Res* 37(4):710–719
- Rott H, Scheuchi B, Siegel A, Grasemann B (1999) Monitoring very slow slope movements by means of SAR interferometry: a case study from a mass waste above a reservoir in the Otztal Alps, Austria. *Geophys Res Lett* 26(11):1629–1632
- Saha AK, Gupta RP, Sarkar I, Arora MK, Csaplovics E (2005) An approach for GIS-based statistical landslide susceptibility zonation- with a case study in the Himalayas. *Landslides* 2:61–69
- Singleton A, Li Z, Hoey T, Muller JP (2014) Evaluating sub-pixel offset techniques as an alternative to D-InSAR for monitoring episodic landslide movements in vegetated terrain. *Remote Sens Environ* 147:133–144
- Small D, Werner CL, Ndesch D (1993) Baseline modelling for ERS-1 SAR Interferometry. In: Proceedings of the international geoscience and remote sensing symposium (IGARSS'93), 18–21 August, 1993, Tokyo, vol 3, pp 1204–1206
- Squarzon C, Delacourt C, Allemand P (2003) Nine years of spatial and temporal evolution of the La Valette landslide observed by SAR interferometry. *Eng Geol* 68:53–66
- Strozzi T, Luckman A, Murray T, Wegmüller U, Werner CL (2002) Glacier motion estimation using SAR offset-tracking procedures. *IEEE Trans Geosci Remote Sens* 40(11):2384–2391
- Vöge M, Frauenfelder R, Ekseth K, Arora MK, Bhattacharya A, Bhasin RK (2015) The Use of SAR Interferometry for Landslide Mapping in the Indian Himalayas. In: The international archives of the photogrammetry, remote sensing *and* spatial information science, XL-7/W3, pp 857–863. doi:[10.5194/isprsarchives-XL-7-W3-857-2015](https://doi.org/10.5194/isprsarchives-XL-7-W3-857-2015)
- Wright TJ, Parsons BE, Jackson JA, Haynes M, Fielding EJ, England PC, Clarke PJ (1999) Source parameters of the 1st October 1995 Dinar (Turkey) earthquake from SAR interferometry and seismic body-wave modeling. *Earth Planet Sci Lett* 172(1–2):23–37
- Yin Y, Zheng W, Liu Y, Zhang J, Li X (2010) Integration of GPS with InSAR to monitoring of the Jiaju landslide in Sichuan, China. *Landslides* 7:359–365